Climate Data Record (CDR) Program

Climate Algorithm Theoretical Basis Document (C-ATBD)

Special Sensor Microwave/Imager Sounder (SSMIS)

V2 Brightness Temperature – CSU

Special Sensor Microwave/Imager Sounder (SSMIS)

V2 Brightness Temperature – CSU Gridded

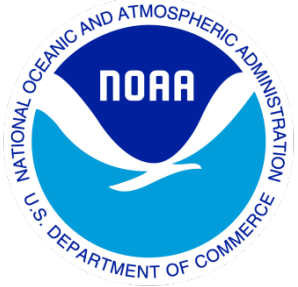

CDR Program Document Number:	CDRP-ATBD-0338
Configuration Item Number:	01B-15 and 01B-15a
Dataset Version/Revision:	V02R00
Revision 3:	June 16, 2021

REVISION HISTORY

Rev.	Author	DSR No.	Description	Date
1	Wesley Berg, Colorado State University	DSR-393	Initial Submission to CDR Program	07/12/2013
2	Wesley Berg, Colorado State University	DSR-924	Addition of daily gridded FCDR and ICDR brightness temperature data files	4/15/2015
3	Wesley Berg, Colorado State University	DSR-1581	Updates for FCDR Version 2 release (V02R00)	6/16/2021

TABLE of CONTENTS

LIST of FIGURES

LIST of TABLES

1. Introduction

1.1 Purpose

The purpose of this document is to describe the algorithm used to create the Colorado State University (CSU) Fundamental Climate Data Record (FCDR) of brightness temperature data from the Special Sensor Microwave Imager Sounder (SSMIS) instruments currently operating on board the Defense Meteorological Satellite Program (DMSP) spacecraft F16, F17, and F18. The actual algorithm is defined by the computer program (code) that accompanies this document, and thus the intent here is to provide a guide to understanding that algorithm, from both a scientific perspective and in order to assist a software engineer performing an evaluation of the code.

1.2 Definitions

None Currently

1.3 Referencing this Document

This document should be referenced as follows:

SSMIS Brightness Temperature – CSU and SSMIS Brightness Temperature – CSU Gridded - Climate Algorithm Theoretical Basis Document, NOAA Climate Data Record Program CDRP-ATBD-0338 Rev. 3 (2021). Available at http://www.ncdc.noaa.gov/cdr/operationalcdrs.html

1.4 Document Maintenance

Synchronization between this document and the algorithm is achieved through version and revision numbers. The version and revision numbers found on the front cover of this document can be compared with the values of `VERSION` and `REVISION` in the source file `params.h` and in the FCDR filenames and metadata. If the document applies to the algorithm, then these numbers will match. If they don't match and it is found that the document needs to be updated, then the header comment in the file `ssmis_fcdr.c` should be consulted – under its `HISTORY` section is a description of the changes for each version and revision from which the necessary updates to this document can be made.

2. Observing Systems Overview

2.1 Products Generated

The data product generated by this algorithm is the Fundamental Climate Data Record (FCDR) of brightness temperature (Tb) data from the SSMIS sensors, including the five low-resolution environmental sensor channels (Tb19v, Tb19h, Tb22v, Tb37v, Tb37h) and the five high-resolution imager channels (Tb91v, Tb91h, Tb150h, Tb183±1, Tb183±3, Tb183±7), stored in netCDF version 4.0 files that include the necessary metadata and supplementary data fields. In addition to the seven intercalibrated SSM/I equivalent channels and four other imager channels (i.e. 150, 183) listed above, the output FCDR file also contains the Tb and geolocation information for the lower atmospheric sounder (50 – 60 GHz) and upper atmospheric sounder channels (60 – 63 GHz) with limited corrections and no intercalibrated applied. Additionally, a daily gridded version of the FCDR Tb data is produced on a 0.25 x 0.25 degree equal angle global grid. The data fields for both the pixel-level and gridded FCDR data files are described in detail section 3.4.7 below.

2.2 Instrument Characteristics

Data input to this algorithm is from the SSMIS instruments on board the DMSP satellites F16, F17, F18 and F19. The DMSP series satellites are in sun-synchronous polar orbits at an altitude of approximately 833 km. The instrument is a conically scanning passive microwave radiometer sensing upwelling microwave radiation at 24 channels covering a wide range of frequencies from 19 – 183 GHz. Data is collected along an active scan of 143.2 degrees across track producing a swath width on the ground of approximately 1707 km with 12.5 km scene spacing. This configuration is shown in Figure 1. Detailed specifications for the spacecraft and instrument are found in Northrop Grumman (2002).

The channels consist of the following sets: *Environmental sensor* (ENV) – channels 12-16; *Imager* (IMG) – channels 8-11 and 17-18; *Lower atmospheric sounding* (LAS) – channels 1-7 and 24; *Upper atmospheric sounding* (UAS) – channels 19-23. Of these channels, the SSM/I equivalent channels include all of the environmental channels (12-16) and imager channels 17 and 18. The Tb from these seven window channels as well as the 150 and 183 GHz moisture sounding channels (i.e. channels 8-11) are intercalibrated to GPM GMI along with the other DMSP microwave radiometers (i.e. SSM/I and SSMIS). Detailed channel characteristics for all channels are shown in Tables 1-4.

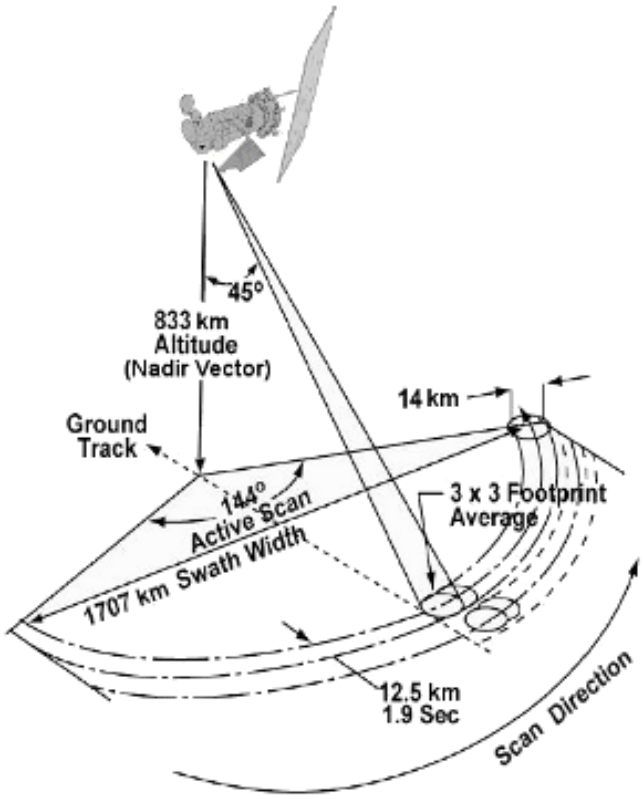

Figure 1: SSMIS Scan Configuration.

Table 1: Intercalibrated window channels (FCDR channels)

Center Frequencies (GHz)	**19.35**	**19.35**	**22.235**	**37.0**	**37.0**	**91.655**	**91.655**
Channel Number	13	12	14	16	15	17	18
Polarization	V	H	V	V	H	V	H
Bandwidth (MHz)	400	400	450	1500	1500	1500	1500
Sensitivity (K)	0.7	0.7	0.7	0.5	0.5	0.9	0.9
EFOV (along track x across track in km)	74 x 45	74 x 45	74 x 45	45 x 28	45 x 28	16 x 13	16 x 13
Sampling Interval (along track x across track in km)	12.5 x 25	12.5 x 25	12.5 x 25	12.5 x 25	12.5 x 25	12.5 x 12.5	12.5 x 12.5

Table 2: Intercalibrated moisture sounding channels (FCDR channels)

Center Frequencies (GHz)	**150.0**	**183.31±1**	**183.31±3**	**183.31±7**
Channel Number	8	11	10	9
Polarization	H	H	H	H
Bandwidth (MHz)	1500	500	1000	1500
Sensitivity (K)	0.88	1.25	1.0	1.2
EFOV (along track x across track in km)	16 x 13	16 x 13	16 x 13	16 x 13
Sampling Interval (along track x across track in km)	12.5 x 12.5	12.5 x 12.5	12.5 x 12.5	12.5 x 12.5

Table 3: Lower atmospheric temperature sounding channels (no intercalibration applied)

Center Frequencies (GHz)	**50.3**	**52.8**	**53.596**	**54.40**	**55.50**	**57.29**	**59.4**
Channel Number	1	2	3	4	5	6	7
Polarization	H	H	H	H	H	RC	RC
Bandwidth (MHz)	400	400	400	400	400	350	250
Sensitivity (K)	0.4	0.4	0.4	0.4	0.4	0.5	0.6
EFOV (along track x across track in km)	27 x 18	27 x 18	27 x 18	27 x 18	27 x 18	27 x 18	27 x 18
Sampling Interval (along track x across track in km)	12.5 x 37.5	12.5 x 37.5	12.5 x 37.5	12.5 x 37.5	12.5 x 37.5	12.5 x 37.5	12.5 x 37.5

Table 4: Upper atmospheric temperature sounding channels (no intercalibration applied)

Center Frequencies (GHz)	**50.3**	**52.8**	**53.596**	**54.40**	**55.50**	**57.29**
Channel Number	19	20	21	22	23	24
Polarization	RC	RC	RC	RC	RC	RC
Bandwidth (MHz)	1.5	1.5	1.5	3.0	8.0	30.0
Sensitivity (K)	2.4	2.4	1.8	1.0	0.6	0.7
EFOV (along track x across track in km)	27 x 18	27 x 18	27 x 18	27 x 18	27 x 18	27 x 18
Sampling Interval (along track x across track in km)	12.5 x 75	12.5 x 75	12.5 x 75	12.5 x 75	12.5 x 75	12.5 x 75

Channel characteristics shown above are from:

- Northrop Grumman (2002), Table 1 (Bandwidth), Table 3 (EFOV, Sampling Interval).
- Kunkee et al. 2008, Table II (Sensitivity).

3. Algorithm Description

3.1 Algorithm Overview

The algorithm operates on input BASE files from F16, F17, F18 and F19, which contain the original antenna temperature (Ta) and calibration data for all 24 channels as input. The input data is processed through several stages for geolocation, pointing and calibration corrections, and intercalibrated brightness temperatures (Tb) are output in the final FCDR files. The processing stages include: calculate spacecraft ephemeris; calculate pixel geolocation; quality control; corrections for solar and lunar intrusions into the warm load and cold sky mirror; cross-track bias correction; conversion of antenna to brightness temperatures via an antenna pattern correction; correction for heating and solar intrusion biases associated with sun angle; and finally intercalibration of the window channels (19v, 19h, 22v, 37v, 37h, 91v, and 91h) and the water vapor sounding channels (150h, 183±1, 183±3 and 183±7) to the reference sensor (i.e. GPM GMI) to obtain a physically a consistent Tb record across all of the SSM/I and SSMIS sensors on board the DMSP satellites. Note that many of the processing steps were adapted from the FNMOC operational SSMIS ground processing software, or GPSr9, (see Berg and Sapiano, 2013 for more details) used to produce the SDR Tb files. Several processing steps from the operational code including a Doppler correction, an emissive reflector correction, and a surface dependent antenna pattern correction are included within the FCDR processing code, but they are not used in the V2 SSMIS FCDR processing. These routines are included for documentation purposes as well as future comparisons and development efforts.

3.2 Processing Outline

The steps of this algorithm include reading the input, the above specified sequential processing stages each of which can be turned on or off with a flag, and writing the output data file. Each stage is described in this section. The processing flow is shown in Figure 2.

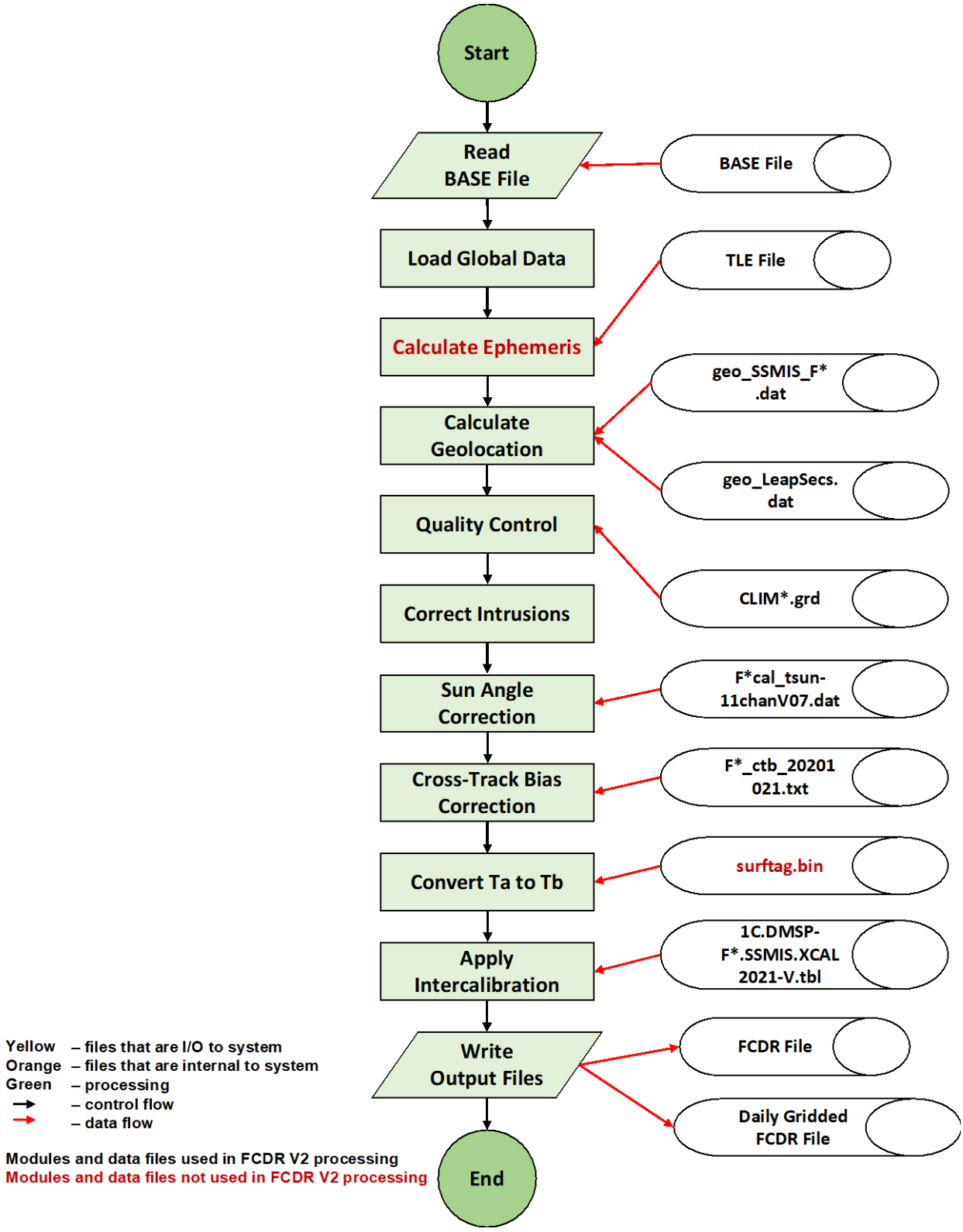

Figure 2: Flowchart for SSMIS version 2 processing

3.2.1 Read Input

Data from the input BASE file (see section 3.3.3), optional Two-Line Element (TLE) files (see section 3.3.2), and look-up tables (see section 3.4.5), is read and stored in global variables that are accessed by the subsequent steps. Space is allocated to store output data and certain fields are prepopulated from the input data.

3.2.2 Calculate Ephemeris

The spacecraft position and velocity have been precomputed from TLE orbital elements files and are stored in the input BASE files. Because the TLE files are not publicly available and cannot be publicly distributed at this time, the algorithm currently uses the precomputed spacecraft position and velocity data stored in the input BASE files. The Simplified General Perturbations (SGP4) code used to compute the spacecraft position and velocity from the TLE files, however, is included as part of the FCDR algorithm package. If TLE files are available, the option to recompute the spacecraft ephemeris is available within the code. For the initial FCDR processing this option was turned off and the position and velocity information stored in the BASE files was used. When this processing stage is turned on, a flag additionally allows a choice between recomputing the ephemeris from the TLE when the time of the TLE is closer than that used in the BASE file or regardless of timing.

3.2.3 Calculate Geolocation

Taking as input the spacecraft position and velocity along with sensor mount angle data and spacecraft orientation data, the geolocation or latitude and longitude of each pixel is calculated and stored. Additional information related to the spacecraft view angles and associated sun angles are also computed. These include the satellite zenith and azimuth angles and solar zenith and azimuth angles, which provide the direction of the satellite and the sun from the normal to the Earth for each pixel. The satellite zenith angle is also referred to as the Earth incidence angle (EIA), which is important for retrieval algorithms as it affects the resulting Tb. The sun glint angle is also computed and provided to identify potential specular reflection from the sun over water surfaces that may also impact retrieval algorithms. Additional information computed at this stage includes angles relating the position of the sun relative to the spacecraft direction of motion, whether or not the spacecraft is in the Earth's shadow, and the time since the spacecraft entered into the Earth's shadow or time since eclipse. Only the EIA and sun glint angles are written out in the FCDR files, but the other angles/fields are computed for analysis purposes and can be output into optional XBASE files. Estimates of the spacecraft/sensor roll and pitch were estimated based on an analysis of simulated minus observed cross-track bias patterns. Offsets in the roll direction result in a slope across the scan while offsets in the pitch direction result in an arc shaped pattern in the cross-track biases. Subsequent coastline analysis, which is described in detail by Berg et al. 2018 and Kroodsma et al. 2021 was used to solve for offsets in the spacecraft/sensor yaw direction along with delta EIA and timing offsets.

There are several important changes in the geolocation/pointing corrections from Version 1 of the FCDR. First, the roll and pitch offsets were computed from the residual slope and arc patterns across the center of the scan between simulated and observed Tb. Previously, the cross-track bias correction included these roll and pitch effects and were based on the pattern in the Ta. Second, yaw, delta EIA and timing offsets were computed based on the coastline analysis. A change in the ½ cone angle, or delta EIA, has a similar impact on the coastline shifts as a change in pitch, however, unlike a pitch offset the ½ cone angle offset does not impact on the cross-track scan bias pattern. This allows for pitch and ½ cone angle offsets to be derived independently. Finally, a timing offset was computed from the coastline analysis, which showed a rather abrupt change in the geolocation in 2011. In version 1, time-dependent roll, pitch and yaw offsets were computed, however, these were not updated for changes past the 2013 V1 delivery leading to errors in the later data record. The single timing offset change now accounts for the time-dependent variations without introducing additional time-dependent biases or requiring regular updates. More information on the geolocation analysis and results is given in Kroodsma et al. 2021.

All five of the sensor offsets (i.e. roll, pitch, yaw, delta EIA and timing) are computed and applied separately for the four different feedhorns containing the FCDR channels. These include ENV1 (19v, 19h and 22v), ENV2 (37v and 37h), IMG1 (150h, 183±1, 183±3 and 183±7) and IMG2 (91v and 91h). The offsets are the same for all the channels within a given feedhorn and are given in the tables 5 and 6 below.

Table 5: Sensor mount offsets by sensor (i.e. F16, F17, F18 and F19) and feedhorn (i.e. ENV1, ENV2, IMG1 and IMG2). Offsets were computed for roll, pitch and yaw directions as well as an offset for the ½ cone angle, or delta EIA. Note that roll and pitch offsets could not be computed for the IMG1 channels due to lack of signal in the cross-track bias patterns.

Feedhorn	Sensor Offset	F16	F17	F18	F19
ENV1 (19v, 19h and 22v)	Roll	0.14	-0.03	0.17	0.00
	Pitch	0.16	0.08	0.06	0.14
	Yaw	0.20	0.19	-0.42	-0.50
	Delta EIA	0.61	0.25	0.34	0.07
ENV2 (37v and 37h)	Roll	0.08	-0.02	0.11	-0.06
	Pitch	0.09	0.03	0.13	0.09
	Yaw	0.26	0.32	-0.62	-0.76
	Delta EIA	0.23	0.17	0.34	0.20
IMG1 (150h, 183±1, 183±3 and 183±7	Roll	0.00	0.00	0.00	0.00
	Pitch	0.00	0.00	0.00	0.00
	Yaw	0.15	0.36	-0.57	-0.57
	Delta EIA	-0.11	-0.33	-0.10	-0.35
IMG2 (91v and 91h)	Roll	0.11	-0.08	0.15	-0.04
	Pitch	0.31	0.26	0.25	0.17
	Yaw	0.31	0.21	-0.31	-0.60
	Delta EIA	0.22	-0.02	0.19	-0.25

Table 6: Timing offsets by sensor. For 16, F17 and F18, there is a distinct change in the pointing, which was attributed to a timing offset. The date of this change is different for each sensor, but they all occurred in 2011. There was no change in the timing offset detected during the short lifetime of F19.

Satellite	Offset	Date Applied	Offset	Date Applied
F16	-0.25	Before October 6, 2011	0.50	Starting October 6, 2011
F17	-0.20	Before July 28, 2011	0.30	Starting July 28, 2011
F18	-0.40	Before May 15, 2011	0.50	Starting May 15, 2011
F19	0.25			

3.2.3.1 Pixel Geolocation (Geodetic Latitude and Longitude)

The process for calculating the pixel latitude and longitude starts with the calculation of the Instantaneous Field-Of-View (IFOV) matrix in sensor coordinates. Several rotations are required to obtain the IFOV in Geocentric Inertial (GCI) coordinates. First there is the sensor-to-spacecraft rotation that obtains the IFOV relative to the spacecraft. Next there is the spacecraft-to-orbital (geodetic nadir pointing) rotation that obtains the IFOV relative to the path of the spacecraft. Finally, there is the orbital-to-GCI rotation that obtains the IFOV in GCI coordinates. With the IFOV in GCI coordinates, the intersection of the IFOV with the oblate spheroid used to model Earth is calculated and this is then used to get geocentric, then geodetic latitude and longitude.

3.2.3.2 Satellite Zenith and Azimuth

In order to calculate the satellite zenith (aka Earth Incidence Angle) and azimuth angles, it is necessary to first determine the local zenith (up), north and east vectors. The satellite zenith angle is the angle between the local up vector and the pointing vector and the azimuth angle is the angle between the projection of the pointing vector on the surface and the local north vector where positive azimuth angle is clockwise when viewed from above.

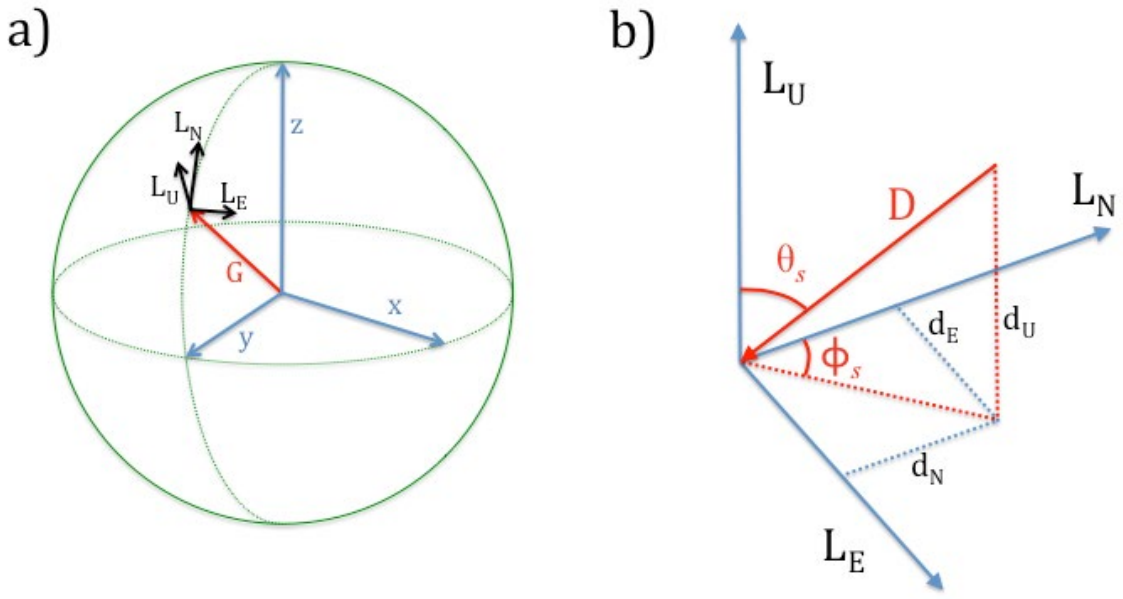

Figure 3: Diagram showing (a) the local zenith (up), east and west vectors on Earth's surface relative to the GCI frame; and (b) the zenith and azimuth angles relative to the pointing vector **D**.

3.2.3.3 Solar Angles

Various solar angles are calculated based on the Sun position vector in GCI coordinates determined as described in Appendix C, section C4 of Sapiano et al. (2010). Solar beta angle, sun glint angle, and solar zenith and azimuth angles are found using the Sun position vector. The time since eclipse is also calculated to provide information on solar heating of the spacecraft based on how long it has been in sunlight or shadow.

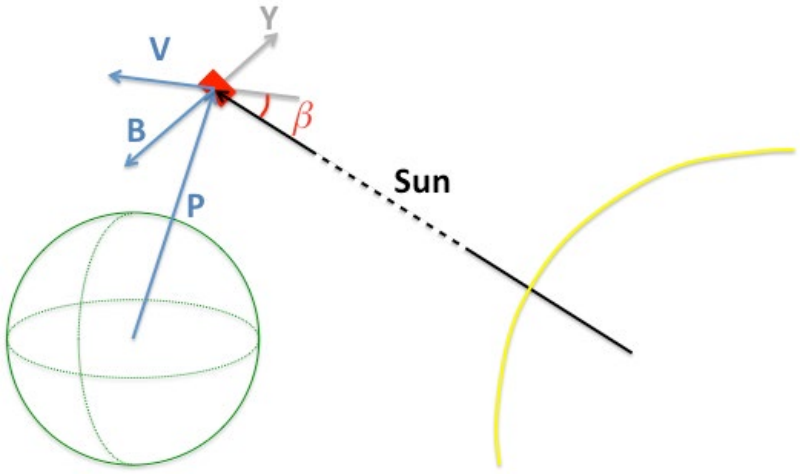

Figure 4: Diagram of angles associated with the solar beta angle.

3.2.4 Quality Control

The quality control processing stage (*qual_control.c*) consists of multiple procedures, which check for potentially erroneous data, correct it if possible, and set the corresponding quality flag. Note that the quality control is done on the input Ta prior to the application of the antenna pattern correction (APC). The quality flag values are specified in the file metadata and are defined in the include file *quality_flags.h*. There is a quality flag value for each scan and pixel, with one flag for each of the six feedhorns (env1, env2, img1, img2, las, and uas). The flag values consist of three categories with a value of zero indicating good data, values between 1 and 99 indicating a warning or caution, and values from 100 and above indicating an error. For pixels with flag values >= 100 the affected Tb are subsequently set to missing. The warning flags provide the user information on potential issues, which are often algorithm dependent. For example, a quality flag value of 1 indicates possible sun glint, which is only an issue over reflective surfaces like water and is not an issue at all for some retrievals. Note that many of the quality control checks are currently only applied to the seven FCDR channels, although basic geolocation and non-physical pixel checks are done for all of the channels. A short description of the various quality control procedures follows. Additional details on the quality control procedures are available in the CSU technical report by Berg and Rodriguez-Alvarez (2013).

3.2.4.1 Check BASE file

Some quality control checks were done during the creation of the BASE files including checks for scan time errors leading to erroneous pixel geolocation. The pixel geolocation check is done for all channels. This routine sets the associated FCDR quality flag and sets the affected output Tb to missing.

3.2.4.2 Check Pixel

Ta values outside of specified minimum (current 50 K) and maximum (currently 350 K) thresholds (i.e. nonphysical) have the appropriate quality flag set and the affected Ta are set to missing. This check is done both on the Ta, as well as the Tb values after the various corrections are applied.

3.2.4.3 Check Environmental Sensor Channels

The climatology check for the environmental channels (i.e. 19v, 19h, 22v, 37v and 37h) was found to produce a significant number of erroneously flagged scans. It was based on a quality check developed for the SSM/I sensors, which had different QC issues. For this reason, this check was turned off in Version 2 of the FCDR.

3.2.4.4 Check Imager Channels

As with the environmental channels, the version 1 climatology check was found to erroneously flag a significant number of scans. The 91v and 91h channels on F16, however, started to exhibit significant scan dependent errors starting on April 24, 2015.

Unfortunately, all of the imager channels including the 150h and 183 GHz channels also exhibited significantly elevated noise (i.e. NEDT) and unphysical Tb at this time. The 91h and 183 GHz channels returned to normal NEDT values as of September 2, 2015. As a result, a new QC check for the 91v channel was developed using the 91h Tb data for the period from September 2, 2015 forward. The 150h channel returned to normal NEDT values slightly early, by August 10, 2015. The 91v quality check is specific to F16 for the period from September 2, 2015 forward.

3.2.5 Solar and Lunar Intrusion Correction

Corrections are applied to the Ta to account for solar and lunar intrusions into the warm load and the cold-sky mirror. The corrections are based on those applied in the SSMIS Ground Processing Software revision 9 (GPSr9) released July 2010. The solar intrusions are corrected by calculating a corrected (FFT smoothed) gain that is used during periods with solar intrusions (note that this gain includes the corrections for lunar intrusions). A single channel is used to detect solar intrusions (91V for F16 and F18; 91H for F17) and the gain for this channel is smoothed using FFT smoothing. A solar intrusion is identified when peaks in the smoothed gain exceed set thresholds and the gain is replaced during these times with a smoothed, interpolated gain. Additional details are available in the CSU technical report on corrections and APC for SSMIS Ta to Tb (Berg and Sapiano 2013).

3.2.6 Cross-track Bias Correction

A significant falloff in the Ta occurs near the left edge of the scan for the 19v, 19h and 22v channels due to an obstruction affecting the side lobes of the antenna pattern. For SSMIS, the 37v and 37h channels also show a significant falloff in the Ta values, but for the right edge of the scan. The edge of scan falloffs are significantly smaller for the imager channels. After the roll and pitch offsets were adjusted and the resulting pattern across the center of the scan was verified to be flat for each of the sensors, a correction for the edge-of-scan falloff was developed based simulated versus observed Tb over oceans (i.e. cold scenes) and vegetated land (i.e. warm scenes). A scale and offset were computed based on a polynomial fit to the scan pattern, which was then subtracted from the observed Tb. This correction accounts for changes in the falloff as a function of the scene temperature, which was not done in version 1. This results in consistent Tb values across the entire scan independent of the scene temperature. Additional details on this correction are provided by Kroodsma et al. 2021.

3.2.7 Ta to Tb Conversion

The SSM/I equivalent channels have both a cross-polarization and spillover correction applied. For the remaining channels only the spillover corrections is applied. Note that in the ground processing software (GPSr9) a surface-dependent antenna pattern correction (APC) is applied for the SSM/I equivalent channels. For climate applications, however, it was determined that tying the APC to the surface type could lead to regional biases and thus the decision was made to use the original cross-pol and spillover corrections and to separately apply a scene-dependent temperature intercalibration.

Additional details are available in the CSU technical report on corrections and APC for SSMIS Ta to Tb (Berg and Sapiano 2013).

3.2.8 Sun-Angle Correction

A number of issues related to the heating and/or position of the sun were found to impact the observed SSMIS Tb on the original F16 spacecraft (Kunkee et al. 2008a, Bell et al. 2008). These include both direct and indirect intrusions into the warm load and an emissive reflector. As noted by Kunkee et al. (2008b), “recent laboratory measurements of other SSMIS flight-unit reflectors have indicated the possibility of extremely low surface electrical conductivities of F-16 (S/N 02) and F-17 (S/N 04) reflectors (e.g., 0.14–0.23 MS/m for S/N 03 and 0.54–1.2 MS/m for S/N 05) compared with pure aluminum (36 MS/m). Further analysis suggests that the low conductivities may be due to excessive surface roughness in combination with insufficient VDA thickness as the likely source of the large reflector emissivity. As part of the F16 Cal/Val team recommendations, procedures to measure the electrical conductivity and emissivity of the reflectors are now part of the preflight readiness analysis for future SSMIS instruments. The main reflector of the third SSMIS instrument (F-18) scheduled for launch in mid-2008 has been replaced with a spare reflector having significantly higher conductivity (17–18.5 MS/m).” Analysis of the emissive reflector issue by Berg and Sapiano (2013) indicates that it is much less of a factor with F18, with the 91 GHz channels on F17 showing the largest impact.

With regard to the issue of solar intrusions into the warm load, prior to the launch of F17 a fence was installed to eliminate direct solar intrusions into the warm load and the temperature sensor on the reflector arm was relocated to the back of the reflector to better characterize the impact of the emissive reflector (Bell et al. 2008). These changes were also made to the SSMIS on board F18, however, in addition a change was made to the reflective cover on the canister top to further reduce solar reflections into the warm load, but subsequently causing the instrument to run hotter and changing the characteristics of the calibration errors (Dave Kunkee, email communication).

As described by Berg and Sapiano (2013), anomalous jumps in the radiometer gain were identified and removed using a Fourier smoothing technique in the operational GPSr9 software. While this correction was implemented in the FCDR code to minimize the effect of these intrusions, it appears there are some residual biases associated with these intrusion events in the Tb data. According to Bell et al. (2008) “Despite the progress made in correcting the data, significant local biases remain in the data: leakage of intrusion affected observations due to inadequacies in the intrusion map, in the region of emergence from the Earth shadow, and an ascending/descending node bias”.

Using observed minus background residuals from data assimilation of the SSMIS Tb, Kunkee et al. (2008b) and Bell et al. (2008) solved for the apparent emissivity of the reflector for each of the channels. While Bell et al. (2008) found effective emissivities close to zero for the SSM/I-like channels, they acknowledged larger uncertainties due to greater errors in the background fields for these channels. A correction for the emissive

reflector was developed for the Universal Preprocessor (UPP) code used for the data assimilation efforts. The emissivity values used in the UPP code are largest for the F17 91 GHz channels with values of 4%, but only 0.5% for the lower frequency window channels. Using double differences with TMI based on the intercalibration approach described by Sapiano and Berg (2013), Berg and Sapiano (2013) attempted to independently solve for the emissivity of the SSM/I equivalent channels. While similar results were found to the UPP values with ~2% for F16 91 GHz, ~2-4% for F17 91 GHz depending on polarization, and lower values for the lower frequency channels, the resulting signal is clearly contaminated by other factors such as the solar intrusions. As a result, it was determined that it is not reasonable to independently solve for the reflector emission.

Instead, Berg and Sapiano (2013) chose to use the double difference approach to solve for Tb biases as a function of the sun angle relative to the direction of motion of the spacecraft. Correction maps, or Tb offsets, as a function of sun azimuth and elevation angles were computed based on matchups with both TRMM TMI and GPM GMI over the entire available time series for each sensor. The resulting maps show very coherent structures, with Tb differences varying as much as 10K for certain sensor/channels depending on the sun position. Details of the sun angle corrections and associated figures are provided in Kroodsma et al. 2021.

3.2.9 Intercalibration

One of the most significant changes to the calibration for Version 2 of the FCDR data is the use of the Global Precipitation Measurement (GPM) Microwave Imager (GMI) as the calibration reference. Pre and post-launch characterization of the GMI calibration have shown it to be extremely well calibrated and stable (Berg et al., 2016; Wentz and Draper, 2016). Previously F13 was chosen as a calibration reference due to its longevity and stable orbit, however, it was recognized that F13 does not represent a high-quality calibration reference in an absolute sense. The intercalibration of the SSMIS sensors relative to GMI is a two-point adjustment based on comparisons over clear-sky oceans (cold scenes) and vegetated land surfaces (warm scenes). Details and results of the intercalibration are provided in Berg et al. 2018 and Kroodsma et al. 2021.

It is important to note that intercalibration does not imply that the resulting Tb will be identical between sensors. Instead, the purpose of the intercalibration is to ensure that measurements between the sensors are “physically” consistent. Physical differences between sensors including diurnal sampling differences and view angle or EIA differences remain and must be accounted for by the geophysical retrieval algorithms.

3.2.10 Write Output

The output FCDR files and daily gridded FCDR files (described in section 3.4.7) containing the final Tb values with corrections and intercalibration applied are written out in NetCDF4. Note that there is an option in the software to write out an XBASE file, which contains all of the data fields in the input BASE file along with the output FCDR variables and the various satellite/sun angles which are computed but not output in the

FCDR file. This option is provided for expert users wanting to further investigate calibration issues etc.

3.3 Algorithm Input

3.3.1 Primary Sensor Data

The raw sensor data are sensor counts from SSMIS instruments. The sensor counts are converted to antenna temperatures (Ta) by applying the calibration from the cold sky and calibration target views each scan and stored in the Temperature Data Record (TDR) files created by the Shared Processing Network Data Exchange Format (SPN DEF). These TDR files are subsequently converted into BASE files, which are used as input for the algorithm and are described in section 3.3.3 below. The original TDR data were obtained and are publicly available from the NOAA CLASS archive.

3.3.2 Ancillary Data

The Two-Line Element (TLE) data created by NORAD containing the satellite orbital elements are used to determine the satellite's position and velocity. The TLE files are in the NORAD TLE format consisting of a title line, which is the satellite name, followed by two lines of formatted text. The use of these files in the FCDR processing is optional, however, as by default the algorithm uses the precomputed spacecraft position and velocity information stored in the input BASE files.

3.3.3 Derived Data

The input data files used for the FCDR processing are referred to as BASE files. These files contain all of the information from the original source TDR files with the following changes/additions. The BASE files have been reorbitized into single orbit granules with duplicate scans removed and spacecraft position and velocity based on the TLE data added (for later use to calculate geolocation). The BASE files are written in NetCDF4 format with metadata added. With the exception of duplicate scans, none of data from the original TDR files is modified or removed. The idea of the BASE files is to preserve the original data in an easy to read self-describing format and to simplify the subsequent FCDR processing. The format of the BASE files is described in detail in the *SSMIS BASE file Format Specification* (http://rain.atmos.colostate.edu/FCDR/Archive_Docs/formatspecs/ssmis_base_format_spec_v1.pdf). Summary statistics of the completeness of the BASE file data record as well as duplicate scans and aggregate error statistics are available in the CSU technical report on quality control (Berg and Rodriguez-Alvarez, 2013).

3.3.4 Forward Models

No forward models are used in the FCDR processing, however, the development of the intercalibration offsets required radiative transfer calculations to account for differences in EIA between sensors. The models used include MonoRTM version 5.3 developed by AER (Clough et al. 2005) for the atmospheric absorption model and the model by

Meisner and Wentz (2012) for ocean emissivities. These models are only used to derive the roll and pitch offsets, the coefficients used in the intercalibration and some of the other corrections.

3.4 Theoretical Description

The software developed for the SSMIS FCDR processing is a stepwise approach described in Section 3.2. This involves reading the input BASE file along with the necessary data coefficient files etc., quality control procedures, calculation of the spacecraft position and velocity (optional) and pixel geolocation, correction for solar and lunar intrusions, application of cross-track bias corrections, APC correction to compute Tb from Ta, correction for sun-angle dependent biases, and application of scene-dependent temperature intercalibration offsets.

3.4.1 Physical and Mathematical Description

3.4.1.1 Physical Background

Passive microwave sensors, such as the SSMIS, measure the microwave radiation emitted by Earth's surface and atmosphere and interacting with the atmosphere through absorption, scattering, and transmission before reaching the sensor. The amount of absorption and scattering of radiation as it travels through the atmosphere depends on the wavelength (or equivalently, frequency) of the radiation and on the state of the atmosphere (e.g. amount of water vapor, rain, cloud, etc.).

The emission of radiation from Earth's surface and atmosphere is described by Planck's blackbody radiation law with the deviation of real materials from ideal blackbodies accounted for by the emissivity (ε) of the material. The brightness temperature (Tb) of a scene retrieved by SSMIS at a frequency depends on the scene's actual temperature:

$$Tb = \varepsilon \, T_{actual} \qquad (1)$$

How the emitted radiation is modified by the atmosphere before reaching the sensor provides information on the state of the atmosphere. Information about carbon dioxide, oxygen, water vapor, liquid water and ice is inferred from SSMIS data by exploiting known changes in the thermal spectrum due to selective absorption, emission, and scattering of radiation. The SSM/I User's Interpretation Guide (Raytheon 2000), section 2, provides theory of remotely sensed electromagnetic radiation – especially microwave radiation – and how it is used to retrieve brightness temperature and other parameters.

3.4.1.2 Astronomical and Geographical Calculations

The Simplified General Perturbations (SGP4) orbital model (Vallado et al., 2006) is used to calculate perturbations of the satellite orbit due to effects of the sun, moon, Earth's oblateness, etc. The orbital position and velocity of the spacecraft calculated using this model are used along with other satellite and sensor parameters (as described in

sections 3.2.3 and 3.4.5.1) to compute the corresponding geolocation or latitude and longitude of each individual pixel or Earth scene.

3.4.1.3 Sensor Characteristics

The physical sensor characteristics and configuration are described in Section 2.2.

3.4.1.4 Simplifications and Approximations

In the quality control processing stage (see section 3.2.4.3), the distance between pixel locations is approximated by using a sphere to model the Earth.

3.4.2 Data Merging Strategy

The original sampling provided by the SSMIS sensors is preserved in the output FCDR data with no merging of the resulting data in either space or time. The resulting FCDR Tb from each of the sensors are intercalibrated to be physically consistent with the observed Tb from the calibration reference sensor (i.e. GPM GMI). Differences between the various sensor Tb due to the local observing time and/or variations in the view angle or EIA remain. Accounting for these differences and merging the data from the various sensors is left to the TCDR developers.

3.4.3 Numerical Strategy

The subroutines to compute the spacecraft position and velocity from the TLE files were implemented based on the North American Aerospace Defense Command (NORAD) SDGP4 code (Vallado et al., 2006). Additional details are provided in the header of the subroutine *sdgp4.c.* Details on the numerical calculations of the pixel geolocation and associated angles are provided in CSU technical report by Sapiano et al. (2010).

3.4.4 Calculations

Details on the processing steps involved in the algorithm are provided in Section 3.2. Additional details are provided in a series of CSU technical reports (Sapiano et al. 2010; Sapiano and Berg 2012; Sapiano and Berg 2013; Berg and Sapiano 2013) and in journal publications (Berg et al. 2016; Berg et al. 2018; Kroodsma et al. 2021).

3.4.5 Look-Up Table Description

Several stages of the algorithm use data that has been calculated and is stored in static look-up tables. The look-up tables used in each stage are described in this section.

3.4.5.1 Calculate Geolocation

The geolocation calculation makes use of the look-up tables contained in the three text files listed below where `F**` is the satellite designation F16 through F19:

1. `geo_SSMIS_F**.dat` – This file contains data lines which are pairs of a variable name and its value for a variety of time, geometry, sensor alignment, and spacecraft attitude variables. For F16, F17 and F18 there are two versions of this file, which contain different timing offsets as described in section 3.2.3 above. The file with the timing offset for the period before the 2011 cuttoff is labeled F1[678]a, while the file for the period after the cuttoff in Table 6 is labeled F1[678]b. F19 has a single file for the full data record.

2. `geo_LeapSecs.dat` – This file contains a line for each leap second adjustment since 1972 giving values for the Julian day, number of seconds, and sign of adjustment. This data is needed to convert between International Atomic Time (TAI) seconds and Universal Time (UT) seconds.

The geolocation code requires values for satellite and sensor parameters (satellite attitude, sensor alignment, elevation offset and scan angle offset) which are stored in the files `geo_SSMIS_F**.dat`. Elevation angle is known for all satellites and so the published values are used (Poe et al. 2008). For scan angle offset, sensor alignment, and satellite attitude, values are determined from the data by the method described in in Section 3.2.3 and by Kroodsma et al. 2021.

3.4.5.2 Solar and Lunar Intrusion Correction

Corrections to the gain are made for solar and lunar intrusions into the warm load and the cold-sky mirror. The Ta values are recomputed based on the adjusted gain values and the quality flag is set indicating that the data have been corrected for an intrusion. Additional details are provided by Berg and Sapiano (2013).

3.4.5.3 Cross-track Bias Correction

The cross-track bias correction coefficients for each satellite are stored in the binary files `F**_ctb_20201021.txt` where `F**` is the satellite designation such as `F16`. These files contain the correction coefficients, both a scale and offset to account for scene-temperature dependent changes, for each scan position for each channel.

3.4.5.4 Ta to Tb Conversion

The spillover and cross-pol coefficients used to compute the Tb values are stored in the files `CorCoefs_SSMIS_F**.dat`.

3.4.5.5 Intercalibration

The Tb calibration offsets used for intercalibration between the different satellites are stored in the text file `1C.DMSP-F**.SSMIS.XCAL2021-V.tbl`, where `F**` is the satellite designation (e.g. F16). The intercalibration files were derived by the NASA XCAL intercalibration team and are the same as those used for the SSMIS intercalibration of the V07 NASA Level 1C dataset (Berg et al. 2016; 2018, Kroodsma et al. 2021). This was done to provide consistency in the Tb between the NASA Level 1C

and NOAA FCDR datasets for the SSMIS sensors. Both datasets rely on corrections developed by both the NOAA FCDR development effort as well as the NASA Precipitation Measurement Missions (PMM) XCAL intercalibration working group. This ensures the application of the best possible corrections for these sensors and to provide consistency to users of both the Level 1C and FCDR data.

The intercal table consists of a number of tie points for each channel with two lines corresponding to each of the 24 channels. The first line for each channel contains a number of temperature values, which correspond to a series of tie points. The second line for each channel contains the calibration difference corresponding to each scene temperature tie point. The calibration delta is interpolated between adjacent tie points with scene temperatures below the lowest tie point temperature or above the highest tie point temperature assigned the corresponding calibration value for those tie points. As a result, there is no extrapolation for low or high scene temperatures beyond the range of available intercalibration information. Only the FCDR channels currently have tie points specified, with zero tie points indicating no intercalibration applied. The window channels (i.e. 19v, 19h, 22v, 37v, 37h, 91v and 91h) have two tie points defined to account for calibration differences over cold and warm scenes. The sounder channels (i.e. 150h, 183±1, 183±3 and 183±7) have a single tie point (i.e. offset) due to the lack of sensitivity to the surface and thus limited scene temperature variations relative to the window channels.

3.4.6 Parameterization

The antenna pattern correction or APC is a parameterization of the measured antenna pattern. Details are provided by Berg and Sapiano (2013).

3.4.7 Algorithm Output

For each input BASE file, the algorithm produces an output FCDR file in NetCDF4 format. There are approximately 15 files per sensor per day and each file is approximately 26 Mbytes. Empty files containing only global metadata fields are produced for orbits with no available input TDR data. The FCDR file contains the final intercalibrated Tb for each SSM/I equivalent channel along with pixel latitude and longitude, time for each scan, spacecraft position, quality flags, sun-glint angle, and fractional orbit number with the necessary metadata and supplementary data fields. A total of six sets of variables are provided, each corresponding to a separate feed horn on the instrument. These include env1 (19v, 19h, and 22v), env2 (37v and 37h), img1 (150h, 183±1, 183±3 and 183±7), img2 (91v, and 91h), las (lower atmospheric sounding channels), and uas (upper atmospheric sounding channels). The data are truncated to the nearest 0.001 degree for the lat/lon values and to the nearest 0.01 K for the Tb and view angles. Internal NetCDF data compression is used to compress the files.

Daily gridded FCDR files are also produced. These files contain Tb values for the eleven FCDR channels (i.e. 19v, 19h, 22v, 37v, 37h, 91v, 91h, 150h, 183±1, 183±3, 183±7) gridded on a global equal angle grid at 0.25 by 0.25 degree resolution. Separate grids are produced for the ascending and descending scans. At higher latitudes where

multiple swaths can overlap during the course of the day, the grid only contains values from the most recent (or latest) overpass values. In addition to the gridded Tb values for the eleven FCDR channels, the view angle or Earth Incidence Angle (EIA), time-of-day (hour, minute and second), and number of pixels in the grid box are provided for each channel and grid point. Note that data are not interpolated at high latitudes to fill missing boxes within the scan, but are replicated from the nearby pixel values.

A detailed specification of the format of the FCDR files is provided in the *SSMIS FCDR File Format Specification*. (http://rain.atmos.colostate.edu/FCDR/Archive_Docs/formatspecs/ssmis_fcdr_format_spec_v1.pdf) Note that the format for the V1 and V2 FCDR files is the same.

4. Test Datasets and Outputs

4.1 Test Input Datasets

No test datasets were used to characterize the algorithm performance. Validation of the resulting FCDR data is described in Section 5.5.

4.2 Test Output Analysis

4.2.1 Reproducibility

As with the version 1 intercalibration (Sapiano et al. 2012, 2013), multiple intercalibration approaches were used to check for consistency and provide an estimate on the residual uncertainties (Berg et al. 2016; 2018, Kroodsma et al. 2021).

4.2.2 Precision and Accuracy

The calibration accuracy of the SSM/I Tb is tied to that of the reference sensor (i.e. GPM GMI), which has been shown to be extremely well calibrated (Wentz and Draper, 2016), within 0.5 K absolute for all channels. While uncertainties in the intercalibration estimates vary by channel and scene temperature, it is generally within ~1.0 K for all channels.

4.2.3 Error Budget

The intercalibration offsets applied in the processing stage described in section 3.2.9 were found as the means over five different techniques, and the standard deviations of the same values provide a measure of the error in the intercalibration. Additionally, uncertainty in the sun-angle correction was calculated, which accounts for residual errors due to solar intrusions, emissive reflector, and other instrument heating errors.

Error Source	**Error Magnitude**
Sensor Noise	0.5 – 0.9 K
Solar Correction	0.5 – 1.3 K
Intercalibration	0.5 K
Absolute Calibration	0.5 K

Table 7: Error Budget

5. Practical Considerations

5.1 Numerical Computation Considerations

This algorithm doesn't use parallelization. No problems with matrix inversions are expected. Failure of the geolocation algorithm to produce a valid latitude and longitude can lead to missing pixel geolocation in rare instances. There are round-off errors in computations and conversions between different data types, which are expected and within the tolerance of the algorithm.

5.2 Programming and Procedural Considerations

The code implementing this algorithm uses standard procedural programming constructs such as: user-defined data structures to manage input and output data fields; control structures; functions; etc. No unusual programming techniques or optimizations are used as ease of maintainability was an important design criterion. Specific features of the code include:

- A pattern used throughout much of the code is to loop through all the scans of an orbit granule and for each scan to loop through the environmental sensor channels, the imager channels, the LAS channels, and the UAS channels and for each of these sets of channels, to loop through all pixels and all channels.
- Each of the eight sequential processing stages of the algorithm can be turned on or off with a flag (these stages are described in section 3.2). This is useful for comparison and validation of individual processing stages.
- Error and exception conditions are handled by direct checking of conditions/return codes in the main control flow, not by a language-supported exception construct.
- For efficiency (both execution speed and working storage space), extensive use of global variables is made.
- The source code is expected to build, and the resulting program to run, on a considerable range of different platforms. For more information on this, see section 5.6.

5.3 Quality Assessment and Diagnostics

See discussion on Section 5.5 on Validation. This includes application of geophysical retrievals and comparisons with other SSM/I FCDR datasets.

5.4 Exception Handling

Error and exception conditions are handled by direct checking of conditions/return codes in the main control flow rather than by a language-supported exception construct.

5.4.1 Conditions Checked

The following conditions identify errors that necessitate that the program terminate. They are trapped and the program prints a suitable message, then exits gracefully with a non-zero status indicating the type of error.

- If an incorrect number of arguments are supplied to the program, a usage message is printed and it exits with status 1.
- If there is an error opening or reading an input file, the program prints an error message and exits with status 1.
- If there is an error creating or writing to an output file, the program prints an error message and exits with status 2.
- If there are unrecoverable errors in the SGP4 orbital model code, an error message is printed and the program exits with status 5.

The following exceptions are trapped and recovered from by skipping over the item that can't be processed, setting codes to track this, and continuing processing with the next item:

- In the geolocation code, where a vector is expected to intersect the oblate spheroid that models the Earth, the solutions of the equation are checked and if the expected intersection doesn't exist, then the relevant data fields are set to missing and the geolocation is skipped over.

5.4.2 Conditions Not Checked

The following possible error condition is not checked for:

- In the unlikely event that the program would run out of memory, it would crash.

5.4.3 Conditions Not Considered Exceptions

Where data fields are missing or do not satisfy quality control checks (described in section 3.2.4), quality flags are set and for those quality issues classified as serious the corresponding data fields are set to indicate missing data. All corrections/conversions are applied only to non-missing data and if any processing stage identifies certain data as missing, it remains missing for all future processing stages. This is considered normal processing and not an exception condition.

5.5 Algorithm Validation

5.5.1 Validation during Development

The following methods were employed to validate the resulting FCDR data.

1) Visual inspections and verification of the various corrections applied to the data. As detailed by Berg et al. 2013 and Kroodsma et al. 2021, to verify the pixel geolocation, monthly images of gridded ascending minus descending Tb maps were checked using the final roll, pitch, yaw, delta EIA and timing offset values for each sensor and compared to maps based on the original TDR data. The results show consistent improvement.

2) Implementation of multiple intercalibration approaches. The use of multiple approaches was done to check for consistency between independent calibration techniques and to provide an estimate of the residual uncertainties. Differences tend to be larger for warm scenes, but are generally quite consistent.

3) Application to geophysical retrievals. We are working with several different thematic CDR or TCDR developers to use the CSU FCDR with their algorithms. That effort is ongoing, but since the ultimate measure the FCDR is the consistency of the TCDRs or geophysical retrievals, we will continue to work to solicit feedback from various communities. We have also run two different in-house retrieval algorithms to test the consistency of the SSMIS FCDR. Figure 5 shows time series of TPW, ocean wind speed, and cloud liquid water over oceans from the complete SSM/I and SSMIS data record. This retrieval over non-precipitating ocean scenes is based on an optimal estimation approach developed by Elsaesser and Kummerow (2008). While the current implementation of this algorithm is not independently validated as a TCDR, it is physical retrieval that accounts for changes in EIA between sensors and is very sensitive to calibration differences, making it a useful tool for analyzing the consistency of the FCDR data record. Finally, the latest operational GPROF precipitation retrieval algorithm (Kummerow et al. 2001, 2011) has been applied to the SSMIS FCDR. Both the non-raining and raining time series show some differences, but it is important to remember that the four DMSP spacecraft with SSMIS sensors have different local observing times that drift/decay over time leading to diurnal cycle differences. A comparison of GPROF rainfall estimates based on coincident overpasses with TRMM TMI indicates mean rainfall differences between the SSMIS sensors and with TMI of less than 3%. Agreement between the SSMIS sensors and GMI is slightly better with differences of less than 1%. The sun angle and associated heating issues are a significant issue for the SSMIS sensors and most problematic for F17 and best for F18.

4) Comparisons with independent FCDRs including the RSS V7 FCDR for F17. We are also working with members of the GPM XCAL team and researchers at the CM-SAF

in their development of an SSMIS FCDR to identify problems and improve upon existing corrections etc.

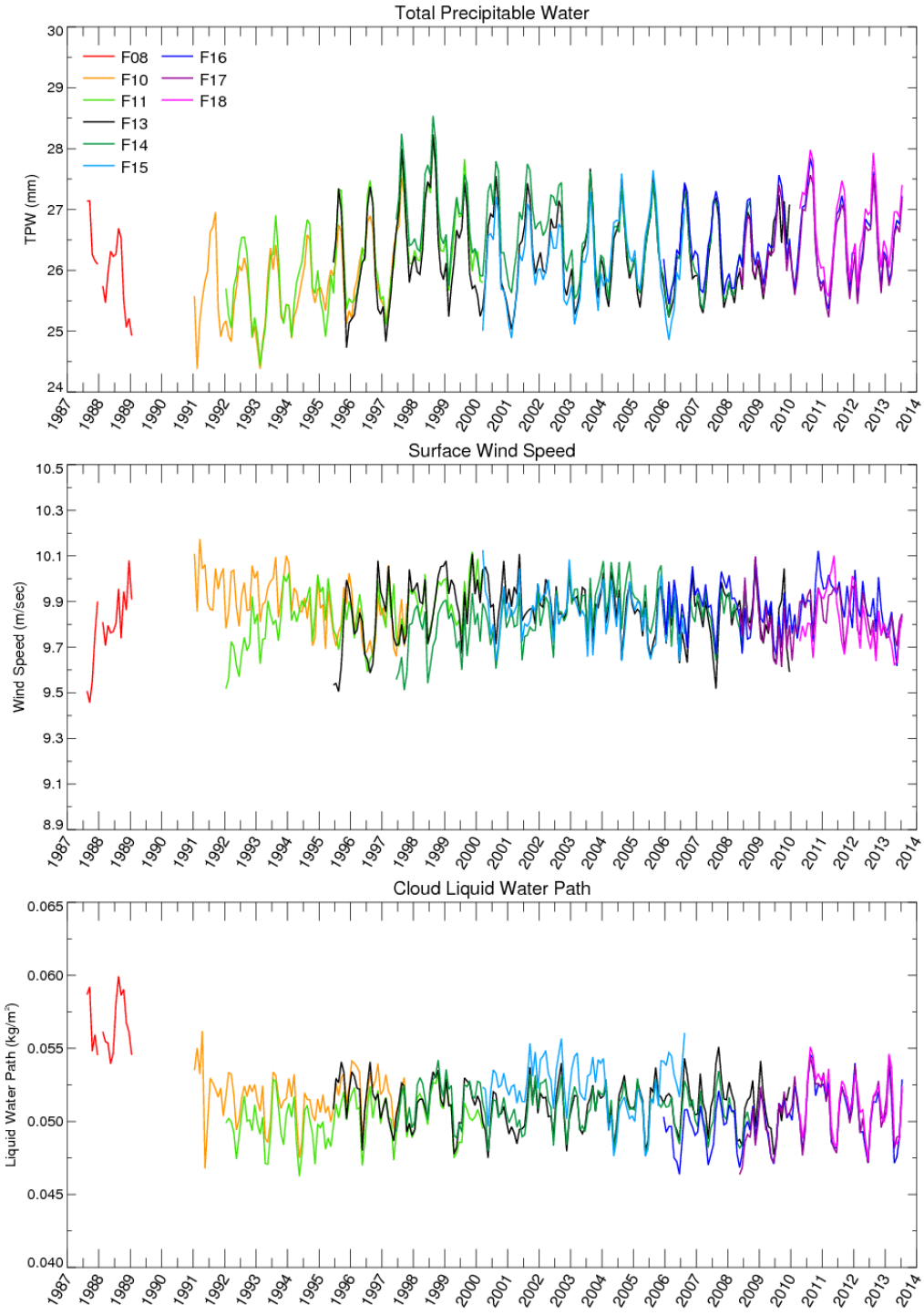

Figure 5: Time series of a) total precipitable water, b) ocean surface wind speed, and c) cloud liquid water path based on the nine DMSP sensors comprising the SSM/I and SSMIS FCDR.

5.6 Processing Environment and Resources

The code was originally developed and run in a processing environment described by the features listed in Table 8.

Hardware	Dell PowerEdge Server
Memory	64GB
Processor	18 dual core Intel Xeon CPU E5-2695 @ 2.1 GHz (Hyperthreading enabled so appears as 72 CPUs)
Operating system	CentOS Linux release 8 (64-bit)
Programming language	C
Compiler	icc (64-bit)
External libraries	hdf5, netcdf, mfhdf, df, hdf5_hl, jpeg, z, imf

Table 8: Processing Environment

The code has been designed to facilitate running it on different platforms by means of the following methods:

1. The Makefile which controls the build process, including compiling and linking.

2. The majority of the code is platform-independent.

3. The platform-dependent parts of the code are separated from the rest and found in the file `sgdp4h.h`. This file contains code to:

    a. Detect the platform;
    b. For functions that will be used from platform-dependent built-in libraries, load the relevant libraries;
    c. Handle the precision differences of data types on different platforms.

To build the code in a new environment, follow these steps:

1. Ensure that the required external libraries listed in Table 8 are installed (for hdf, netcdf, jpeg, z, imf).

2. Examine the Makefile and set the compiler command if different for the new environment. Also comment/uncomment lines if necessary to select 32-bit or 64-bit environments.

3. Run the make command to create the executable program `ssmis_fcdr` from the source code.

Performance:

1. Using a single CPU on the system detailed above takes approximately 8 seconds wall clock time to run a single file.

2. Using approximately ten processors the entire SSMIS FCDR data record can be reprocessed within a couple of days.

3. No temporary storage is required to run the algorithm. The only storage required is for the input and output files. The software with the necessary correction files etc. is less than 200 Mbytes.

6. Assumptions and Limitations

6.1 Algorithm Performance

Near real-time monitoring of the input Ta and corresponding calibration data are provided on the web site (http://rain.atmos.colostate.edu/FCDR). Other than this, however, there is no near real-time assessment of the data and thus the quality of the output FCDR data is dependent on the quality of the input TDR data. As such, the near real-time data is labeled as an interim climate data record (ICDR) instead of an FCDR indicating that it has not been fully vetted for climate applications. Every 6-12 months we will transition this to FCDR status once we have had a chance to run geophysical retrievals and look at the resulting data in more detail.

6.2 Sensor Performance

The sensitivity of the SSMIS instruments is shown in Table 1 and varies from 0.5 to 0.9K for the SSM/I equivalent FCDR channels. As detailed in the report by Berg et al. 2013, Kunkee et al. 2008, and Bell et al. 2008, there are significant issues with the sensor performance due to a variety of issues including warm load intrusions and an emissive reflector. While we have attempted to correct for biases due to spacecraft/instrument heating and intrusion issues, significant transient errors remain along with larger uncertainties corresponding to warm scenes and very cold scenes.

7. V2 Enhancements

Several enhancements were implemented for the V2 FCDR processing.

7.1.1 Intercalibration reference sensor

The original V1 FCDR dataset included a relative intercalibration correction using DMSP F13 as the reference. This was done since there was no community consensus regarding an absolute calibration reference for microwave sensors. Since then, the launch and Cal/Val of the GPM GMI instrument have shown it to be extremely well calibrated and stable for all channels, which includes corresponding channels for all of the SSMIS ENV (19v, 19h, 22v, 37v and 37h) and IMG (91v, 91h, 150h, 183±1, 183±3 and 183±7) channels.

7.1.2 Cross-track bias corrections

The cross-track bias corrections were updated to include the impact of physical Tb variations across the scan due to roll and pitch variations in the spacecraft attitude. The correction to the edge-of-scan falloff was updated based on both cold and warm scene analysis to provide consistent Tb across the scan regardless of scene temperature.

7.1.3 Geolocation

Updated geolocation and EIA values based on improved roll and pitch sensor mount offsets from scan bias patterns along with updated pitch, yaw, delta EIA and timing offsets. The elimination of time-dependent pointing offsets due to the one time change in a timing offset in 2011 should result in much more consistent geolocation and view angle values over the full data record as well as going forward.

7.1.4 Warm scene intercalibration

Both cold and warm-scene intercalibration corrections were developed/applied for the SSMIS window channels.

7.1.5 Sun-angle dependent errors

The sun-angle correction detailed in Berg and Sapiano (2013) was developed to correct for mean errors due to a variety of factors including solar intrusions, emissive reflector, and potentially other calibration errors associated with heating of the hardware. We revisited and made significant updates to this correction, as well as expanding it to include corrections for the 150 and 183 GHz channels.

8. Future Enhancements

Quality control is always an issue that could be improved and given the impact of the emissive reflectors on F16 and F17 potential further improvements should be explored.

The primary goal for future enhancements, however, should be to address issues identified by users.

9. References

Bell, W., et al., 2008: The Assimilation of SSMIS Radiances in Numerical Weather Prediction Models, *IEEE Trans. Geosci. Rem. Sens*., **46**, 884-900.

Berg, W., R. Kroodsma, C. D. Kummerow and D. S. McKague, 2018: Fundamental Climate Data Records of Microwave Brightness Temperatures, *Remote Sensing*, 10, 1306, doi: 10.3390/rs10081306.

Berg, W. et al., 2016: Intercalibration of the GPM Microwave Radiometer Constellation, *J. Atmos. Oceanic Technol.,* 33, 2639-2654, doi: 10.1175/JTECH-D-16-0100.1.

Berg, W., C. Kummerow, M. Sapiano, N. Rodriguez-Alvarez, and F. Weng, A Fundamental Climate Data Record of Microwave Brightness Temperature data from 25 Years of SSM/I and SSMIS Observations, *GEWEX Newsletter*, August 2012.

Berg, W. K. and N. Rodriguez-Alvarez, 2013: SSM/I and SSMIS Quality Control, Technical Report, Colorado State University, http://rain.atmos.colostate.edu/FCDR/.

Berg, W., M. R. P. Sapiano, J. Horsman, and C. Kummerow, 2013: Improved geolocation and Earth incidence angle information for a fundamental climate data record of the SSM/I sensors, *IEEE Trans. Geosci. Rem. Sens.,* 51, 1504-1513.

Berg, W. and M. R. P. Sapiano, 2013: Corrections and APC for SSMIS Ta to Tb, Technical report, Colorado State University, http://rain.atmos.colostate.edu/FCDR.

Clough, S. A. et al, 2005: Atmospheric Radiative Transfer Modeling: A Summary of the AER Codes, J. Quantitative Spectroscopy and Radiative Transfer, 91, 233-244, doi: 10.1016/j.jqsrt.2004.05.058.

Deblonde, G., and S. J. English, 2001: Evaluation of the FASTEM-2 fast microwave ocean surface emissivity model. Tech. Proc. Int. TOVS Study Conf. XI, Budapest, Hungary, WMO, 67**–**78.

Elsaesser, G. S and C. D. Kummerow, 2008: Toward a fully parametric retrieval of the nonraining parameters over the global oceans, *J. Appl. Meteor. Climatol*., 47, 1599-1618.

Kohn, D. J., 1995: Refinement of a semi-empirical model for the microwave emissivity of the sea surface as a function of wind speed. M.S. thesis, Dept. of Meteorology, Texas A&M University, 44 pp.

Kroodsma, R., W. Berg and T. Wilheit, 2021: Updated calibration corrections for V07 of the intercalibrated SSMIS Level 1C data, in prep.

Kummerow, C. D., S. Ringerud, S. Crook, D. Randel, and W. Berg, 2011: An observationally generated a-priori database for microwave rainfall retrievals, *J. Atmos. Oceanic Technol.,* 28, 113-130.

Kummerow, C. D. and Coauthors, 2001: The Evolution of the Goddard Profiling Algorithm (GPROF) for rainfall estimation from passive microwave sensors. *J. Appl. Meteor*., 40, 1801–1820.

Kunkee, D. B., Poe, G. A., Boucher, D. J., Swadley, S. D., Hong, Y., Wessel, J. E., and Uliana, E. A., 2008a: Design and Evaluation of the First Special Sensor Microwave Imager/Sounder. *IEEE Trans. Geosci. Rem. Sens*., **46**, 863–883.

Kunkee, D. B., S. D. Swadley, G. A. Poe, Y. Hong, and M. F. Werner, 2008b: Special Sensor Microwave Imager Sounder (SSMIS) Radiometric Calibration Anomalies – Part I Identification and Characterization, *IEEE Trans. Geosci. Rem. Sens*., **46**, 1017-1033.

Northrop Grumman, 2002: Algorithm and Data User Manual (ADUM) for the Special Sensor Microwave Imager/Sounder (SSMIS). Technical Report 12621, Northrop Grumman, Azusa, California, July 2002. Contract No: F04710-00-C-0001.

Poe, G. A., E. A. Uliana, B. A. Gardiner, T. E. vonRentzell, and D. B. Kunkee, 2008: Geolocation Error Analysis of the Special Sensor Microwwave Imager/Sounder, *IEEE Trans. Geoscl. Rem. Sens*., **46**, 913-922.

Raytheon Company. Special Sensor Microwave/Imager (SSM/I) User's Interpretation Guide, UG32268-900, Revision C, 29 Nov 2000.

Rosenkranz, P. W., 1998: Water vapor microwave continuum absorption: A comparison of measurements and models. *Radio Sci*., **33**, 919–928.

Sapiano, M. R. P. and W. Berg, 2013: Intercalibration of SSM/I and SSMIS for the CSU FCDR, Technical Report, Colorado State University, http://rain.atmos.colostate.edu/FCDR.

Sapiano, M. R. P. and Berg, W. K., 2012: Estimation of Satellite Attitude for SSM/I and SSMIS Geolocation. Technical Report, Colorado State University, http://rain.atmos.colostate.edu/FCDR/.

Sapiano, M. R. P., Berg, W. K., McKague, D. S., and Kummerow, C. D., 2013: Towards an Intercalibrated Fundamental Climate Data Record of the SSM/I Sensors, *IEEE Trans. Geosci. Remote Sens.*, 51, 1492-1503.

Sapiano, M. R. P., Bilanow, S., and Berg, W., 2010: SSM/I and SSMIS Stewardship Code Geolocation Algorithm Theoretical Basis. Technical Report, Colorado State University, http://rain.atmos.colostate.edu/FCDR/.

Vallado, D. A., Crawford, P., Hujsak, R., and Kelso, T. S., "Revisiting Spacetrack Report #3," presented at the AIAA/AAS Astrodynamics Specialist Conference, Keystone, CO, 2006 August 21–24.

Wentz, F. and D. Draper, 2016: On-orbit Absolute Calibration of the Global Precipitation Mission Microwave Imager, *J. Atmos. Ocean. Technol.,* 33, 1393-1412, doi: 10.1175/JTECH-D-15-0212.1.

Wilheit, T. T., 1979a: A model for the microwave emissivity of the ocean's surface as a function of wind speed. *IEEE Trans. Geosci. Electron.,* 17, 244–249.

Wilheit, T. T., 1979b: The effect of wind on the microwave emission from the ocean's surface at 37 GHz., *J. Geophys. Res*., 84, 4921-4926.

Appendix A. Acronyms and Abbreviations

Acronym or Abbreviation	Definition
ANSI	American National Standards Institute
APC	Antenna Pattern Correction
C-ATBD	Climate Algorithm Theoretical Basis Document
CDR	Climate Data Record
DMSP	Defense Meteorological Satellite Program
FCDR	Fundamental Climate Data Record
FOC	Full Operating Capability
FNMOC	Fleet Numerical Meteorology and Oceanography Center
GPSr9	SSMIS Ground Processing Software revision 9
ICD	Interface Control Document
IEEE	Institute of Electrical and Electronic Engineers
IOC	Initial Operating Capability
LAS	Lower Atmospheric Sounding
NCDC	National Climatic Data Center
NOAA	National Oceanic and Atmospheric Administration
NRL	Naval Research Laboratory
OAD	Operational Algorithm Description
SDR	Sensor Data Record (contains Tb data)
SGP4	Simplified General Perturbations orbital model
SSM/I	Special Sensor Microwave/Imager
SSMIS	Special Sensor Microwave Imager/Sounder
TA	Antenna Temperature
TB	Brightness Temperature
TDR	Temperature Data Record (contains Ta data)
TLE	Two Line Element
UAS	Upper Atmospheric Sounding